C Journal of Carbon Research

MDPI

Article

One-Stage Synthesis of Microporous Carbon Adsorbents from Walnut Shells—Evolution of Porosity and Structure

Ilya E. Men'shchikov *, Andrey A. Shiryaev, Andrey V. Shkolin, Alexander E. Grinchenko, Elena V. Khozina, Alexey A. Averin and Anatolii A. Fomkin

Frumkin Institute of Physical Chemistry and Electrochemistry, Russian Academy of Sciences, Leninskii Prospect, 31, bld. 4, 119071 Moscow, Russia; a_shiryaev@mail.ru (A.A.S.); shkolin@phyche.ac.ru (A.V.S.); s-grinchenko@mail.ru (A.E.G.); elena-khozina@rambler.ru (E.V.K.); alx.av@yandex.ru (A.A.A.); fomkinaa@mail.ru (A.A.F.)

* Correspondence: i.menshchikov@gmail.com; Tel.: +7-(495)-952-85-51

Abstract: One-stage synthesis technology for preparing carbon adsorbents with tailored porosity from agricultural waste is worthwhile due to their extensive application value. Thermal gravimetric analysis, low-temperature N_2 adsorption, X-ray diffraction (XRD), small-angle X-ray scattering (SAXS), and Raman spectroscopy were used to record the structure transformations of carbon materials, namely pore development, proceeding in the course of the step-wise pyrolysis of renewable and low-cost raw materials such as walnut shells (WNSs), which was carried out within a temperature range of 240–950 °C in a CO_2 flow. The minimum threshold carbonization temperature for preparing nanoporous carbon materials from WNSs, determined by the examination of the N_2 adsorption data, was 500 °C. The maximum specific micropore volume and BET surface achieved in the process without holding a material at a specified temperature were only 0.19 cm^3/g and 440 m^2/g, respectively. The pyrolysis at 400–600 °C produced amorphous sp^2 carbon. At a temperature as high as 750 °C, an increase in the X-ray reflection intensity indicated the ordering of graphite-like crystallites. At high burn-off degrees, the size of coherently scattering domains becomes smaller, and an increased background in X-ray patterns indicates the destruction of cellulose nanofibrils, the disordering of graphene stacks, and an increase in the amount of disordered carbon. At this stage, pores develop in the crystallites. They are tentatively assigned to crystallites with sizes of 15–20 nm and to micropores. According to the Raman spectra combined with the XRD and SAXS data, the structure of all the pyrolysis products is influenced by the complex structure of the walnut shell precursor, which comprises cellulose nanofibrils embedded in lignin. This structure was preserved in the initial stage of pyrolysis, and the graphitization of cellulose fibrils and lignin proceeds at different rates. Most of the pores accessible for gas molecules in the resulting carbon materials are associated with former cellulose fibrils.

Keywords: adsorption; carbon adsorbent; walnut shell; pyrolysis; porosity; micropores; theory of volume filling of micropores; X-ray analysis; Raman spectroscopy

Citation: Men'shchikov, I.E.; Shiryaev, A.A.; Shkolin, A.V.; Grinchenko, A.E.; Khozina, E.V.; Averin, A.A.; Fomkin, A.A. One-Stage Synthesis of Microporous Carbon Adsorbents from Walnut Shells—Evolution of Porosity and Structure. *C* **2024**, *10*, 79. https://doi.org/10.3390/c10030079

Academic Editors: I. Francis Cheng and Shuguang Deng

Received: 23 July 2024
Revised: 13 August 2024
Accepted: 26 August 2024
Published: 2 September 2024

1. Introduction

It is well known that carbon adsorbents obtained from various nut shells, e.g., coconut shells, meet the requirements for high adsorption activity, production yield, mechanical strength, reactivation, etc.; however, the Russian climate is not suitable for coconut cultivation [1–3]. Walnut shell (*Júglas régia*) is an abundant agricultural waste and is considered a promising low-cost and sustainable feedstock for the production of carbon adsorbents, which are needed for various industrial applications. Approximately 5000 tons of walnut shells (WNSs) are produced each year in Russia [1]. In most of the publications on the synthesis of activated carbons from WNSs, the steam–gas activation of carbonizate in water vapors was preferred [4–7]. The resulting microporous carbon materials have a high density and low ash content, which makes them promising adsorbents for water purification.

The production of activated carbons is carried out in two separate stages, including the (the first stage) carbonization of the carbon-containing precursor at a temperature of 600–800 °C, resulting in an intermediate carbonizate product that was subsequently activated at a temperature of 700–900 °C in the presence of an activating agent (the second stage) [2]. The use of this technique is justified for large volumes of processed raw materials on special technological lines [3]. Nevertheless, for reasons of energy savings, the one-stage synthesis of carbon adsorbents in a CO_2 environment is attracting more and more attention. Within this range of interest, the effect of synthesis parameters such as temperature T_A, the number of stages, and exposure time τ on the adsorption properties of carbon adsorbents prepared from WNSs in the presence of CO_2 was investigated [4–7]. Nowicki and coworkers found that the adsorbents prepared by the one-stage activation of WNSs at T_A = 800 °C in a CO_2 flow had a higher specific surface S_{BET} = 680 m^2/g than a material obtained from a carbonizate produced from the same precursor in an inert argon environment [7]. The authors attributed these findings to the shorter contact with the gas-activating agent. At the same time, Gonzalez et al. showed that an increase in the activation time (τ_A) in the CO_2 flow up to 480 min when the activation temperature rose to 850 °C ensured an increase in the specific BET surface and micropore volume (W_0) of the resulting activated carbons up to 1300 m^2/g and 0.72 cm^3/g, respectively, and the half-width of micropores was ~0.72 nm [6]. Water vapor (steam) is also suggested as an activating agent for use in the synthesis of carbon adsorbents from WNSs [6,8]. For example, carbon material with S_{BET} = 1360 m^2/g and W_0 = 0.74 cm^3/g was prepared by steam activation (τ_A = 60 min, T_A = 850 °C) [6].

Carbon adsorbents from WNSs can also be produced by thermochemical activation with activating agents such as salts (carbonates, sulfates, and nitrates) and acids (sulfuric, nitric, phosphoric, etc.), which release an oxidizing gas (CO_2 and O_2) during a chemical reaction at elevated temperatures ranging from 200 to 650 °C, resulting in highly developed porosity [9–12]. For example, the use of KOH as an activating agent under similar thermal conditions made it possible to prepare the carbon adsorbent with extremely high values of a specific BET surface of 2250 m^2/g and a micropore volume of 1.07 cm^3/g [7]. Yu et al. found that the carbonization of WNSs at 700 °C and subsequential activation at 800 °C in the presence of KOH resulted in carbon adsorbents with highly developed porosity [13]. In addition, they revealed an increase in the specific BET surface from 440 to 1880 m^2/g resulting from the rise in the KOH/carbonizate ratio from 1/1 to 4/1. Activated carbons produced from WNSs using thermochemical activation by $ZnCl_2$ showed good performance in water purification applications [14–16]; a BET surface and micropore volume of 1800 m^2/g and 1.176 cm^3/g, respectively, were achieved [15].

Some researchers used $ZnCl_2$ as an activating agent for the production of activated carbons from WNSs, which showed good performance in water purification applications [14–16]. Yang and coworkers carried out $ZrCl_2$ thermochemical synthesis and prepared activated carbon with a BET surface and micropore volume of 1800 m^2/g and 1.176 cm^3/g, respectively [15].

In general, chemical activation has two main advantages: (1) the high yield of the product (no less than 2 times higher than that of the physical activation) and (2) the uniform and developed microporosity with a high volume [2]. According to the review by Albatrni et al. [17], by now, the thermochemical activation or chemical modification/impregnation of WNSs has been described in 70 percent of publications. Nevertheless, two major drawbacks of thermochemical technology should be noted: (1) a significant amount of wastewater requiring disposal, which reduces the economic attractiveness of the technology and adds to environmental burdens, and (2) serious equipment damage and safety concerns at high temperatures, whose prevention requires the use of corrosion-resistant materials and additional accessory apparatus and chemicals. Therefore, as Albatrni and coworkers pointed out, more and more researchers are emerging who are trying to avoid excessive chemical usage [17]; they employ WNSs without chemical modification and subject the raw material to carbonization in an inert atmosphere followed by physical activation in atmospheric oxidizing gases [18,19]. It should be noted that the adsorbents produced by

physical activation contain a minimum amount of foreign harmful impurities requiring special washing, which significantly expands the scope of their application compared to thermochemical activation products.

It is obvious that activated carbons prepared by physical activation surpass those prepared by the thermochemical method in terms of the simplicity of the technological process and the relatively uniform chemical composition of the final product. Lionetti et al. demonstrated the advantages of a unique apparatus for preparing carbon adsorbents, where the pyrolysis carried out by heating WNSs in nitrogen vapors with a rate of 6 K/min up to 1173 K was followed by physical activation in CO_2 flow at 1173 K [18]. The activation for 90 min made it possible to produce the most efficient adsorbent with the highest content of ultramicropores, which was found to be essential for hydrogen adsorption. Thus, physical activation methods appear to be more important for the production of carbon adsorbents from biomass raw materials, such as WNSs, intended for various applications.

According to the results of the above-mentioned studies [4–7], the temperature range of 750 to 850 °C is the most optimal for the physical activation of agricultural biomass and waste in the CO_2 environment. Notably, activation at these temperatures ensures the most intensive development of adsorbing pores. In addition to the temperature, the duration of activation and the amount of supplied CO_2 are also key factors for producing efficient carbon adsorbents. Since increasing the activation temperature above the specified limits can reduce the synthesis duration and the amount of activating gas, it is necessary to determine the optimal ratio between these factors.

With these considerations in mind, we determined the purposes of the present work as (1) to study the mechanisms of the development of the porosity in the carbon adsorbents prepared from WNSs by one-stage physical activation in CO_2 flow; (2) to examine the adsorption properties of the resulting adsorbents; and (3) to select the optimal operation modes of this synthesis method for producing efficient adsorbents based on the adsorption data. The one-stage activation implies that the activation stage immediately follows the carbonization stage, and the activation temperature T_A coincides with the final temperature of the carbonization process T_C.

2. Materials and Methods

2.1. Preparation of Carbon Adsorbents

Carbon adsorbents were prepared from WNSs obtained from agricultural producers in the southern regions of Russia. The shells were washed in distilled water for 1 h at a temperature of 40 °C and dried in a ventilated oven at a temperature of 60 °C for 12 h. The dried material was broken in a VKMD-10 cone-type crusher. The WNS particles were divided into factions. The fraction of WNS particles with a size ranging from 0.5 to 1.5 mm was selected by sifting through a vibrating sieve. A portion of 250 mg of the crushed shells prepared this way was placed into a ceramic crucible, hung on the rod of a scale, and lowered into the oven chamber of a TGA Q500 thermogravimetric analyzer (TA Instruments, New Castle, DE, USA). The experiment started at an ambient temperature of about 20 °C.

Carbon dioxide produced according to State Standards 8050 (99.8% vol.) [20] was used as an activating agent. It was supplied to the oven chamber at a rate of 60 mL/min throughout the experiment. A similar principle of obtaining activated carbons was used in works [18,19].

Two series of carbon adsorbents, CW (carbonized walnut shells) and AW (activated walnut shells), were prepared in order to examine the mechanism of pore formation during one-stage synthesis. Figure 1 schematically presents the process of the preparation of carbon adsorbents of both series in the oven chamber during heating.

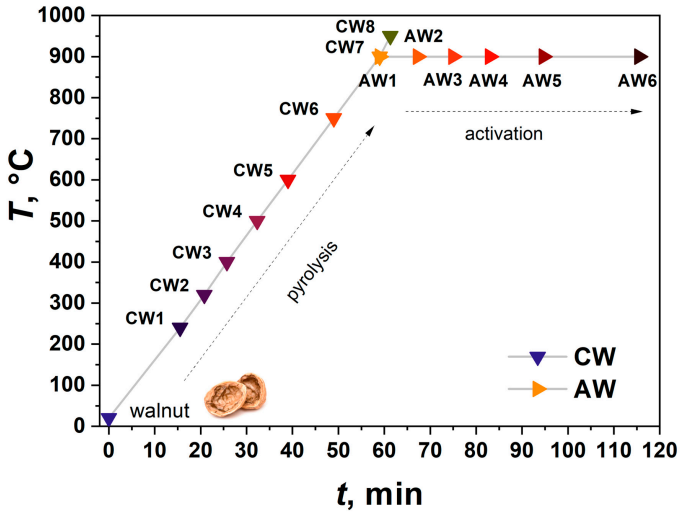

Figure 1. Diagram of obtaining carbon adsorbents of CW and AW series in temperature conditions of processing WNS particles. The transition of the color of the symbols representing CW1–CW7 samples from violet to orange indicates an increase in pyrolysis temperature, and the color changes from orange to black in the AW series show an increase in degree of burn-off. The dark green symbol shows the CW8 sample, which was not further activated.

The CW adsorbents were produced by the pyrolysis of the WNS precursor in CO_2 flow, when the temperature in the chamber rose continuously from room temperature to 240, 320, 400, 500, 600, 750, 900, and 950 °C at a rate of 15 °C/min without isothermal exposure, i.e., once the set temperature was reached, the heating was turned off, and the resulting samples were removed. The designations of the samples shown in the diagram in Figure 1, CW1–CW8, correspond to eight temperatures in the interval of 240–950 °C.

The AW adsorbents were produced by the pyrolysis of the WNSs in CO_2 flow when the temperature in the chamber rose up to T_C = 900 °C at a rate of 15 °C/min with subsequent isothermal exposure at $T_A = T_C$ over a period of time to achieve a certain degree of burn-off δ ranging from 10 to 70 wt.% with respect to the initial mass of the carbonizate. This process was a simulation of the one-stage synthesis of carbon adsorbents. Once a certain value of δ was achieved, the heating was turned off, and the samples were removed from the chamber. It should be noted that the carbonization temperature of 900 °C was selected as optimal for the preparation of a WNS-derived carbon adsorbent with highly developed microporosity since higher temperatures do not result in improved micropore parameters [6,21]. The designations of the samples shown in the diagram in Figure 1, AW1–AW6, correspond to six values of δ, 0, 10, 20, 30, 45, and 70%.

All adsorbents were in the form of coarse powder with a granule size of up to 1 mm.

2.2. Low-Temperature Nitrogen Vapor Adsorption

The porosity characteristics of the prepared carbon adsorbents were evaluated from the data on nitrogen vapor adsorption at 77 K obtained with the help of a Quantachrome Autosorb iQ surface area analyzer (Quantachrome Instr. (Boynton Beach, FL, USA)). The structure and energy characteristics of the adsorbents, namely, the specific micropore volume W_0, standard characteristic energy of adsorption of benzene vapors E_0, and half-width of micropores x_0, were calculated from the adsorption data on nitrogen adsorption using the theory of volume filing of micropores (TVFM), taking into account the affinity coefficient for nitrogen and standard vapor benzene β = 0.33 [22].

The specific BET surface was calculated using the Brunauer–Emmett–Teller (BET) equation [23]. The total pore volume W_S was calculated from the amount of nitrogen adsorbed at P/P_0 = 0.99. The mesopore volume W_{ME} was calculated as the difference $W_{ME} = W_S - W_0$. The specific mesopore surface S_{ME} was calculated using the Kelvin equation [24]. Quenched Solid Density Functional Theory [25], which takes into account

the inhomogeneity of surface geometry, was applied to determine the pore size distribution in the prepared adsorbents.

2.3. XRD and SAXS Measurements

The XRD patterns of the adsorbents were acquired on an Empyrean (Panalytical BV) diffractometer in Bragg–Brentano geometry using nickel-filtered CuKα (λ_{Cu} = 0.1542 nm) radiation in a 2θ angular range of 0° to 100° [26].

Small-angle scattering patterns were recorded using a SAXSess diffractometer (Anton Paar). The angular distribution of scattered radiation was studied within a wide range of scattering vectors ($q = 4\pi\sin(\theta)/\lambda$) of 0.1 to 26 nm^{-1} [26]. The samples were measured in vacuum at room temperature in transmission geometry.

2.4. Raman Spectroscopy Measurements

The Raman spectra of the adsorbents were recorded on an inVia Renishaw Reflex spectrometer (Renishaw plc. (Wotton-under-Edge, England, UK)) at two excitation wavelengths of 532 and 785 nm (2.33 and 1.58 eV, respectively) [27]. The laser power on a sample was not more than 0.1 mW. Special attention was paid to monitoring the absence of damage to the sample.

3. Results and Discussion

3.1. In Situ TGA Analysis of Synthesis of Carbon Adsorbents

The transformations of the WNS precursor into the CW materials during the carbonization stage and subsequent synthesis of the AW adsorbents during the activation stage can be followed by examining the TGA curves shown in Figure 2a and b, respectively.

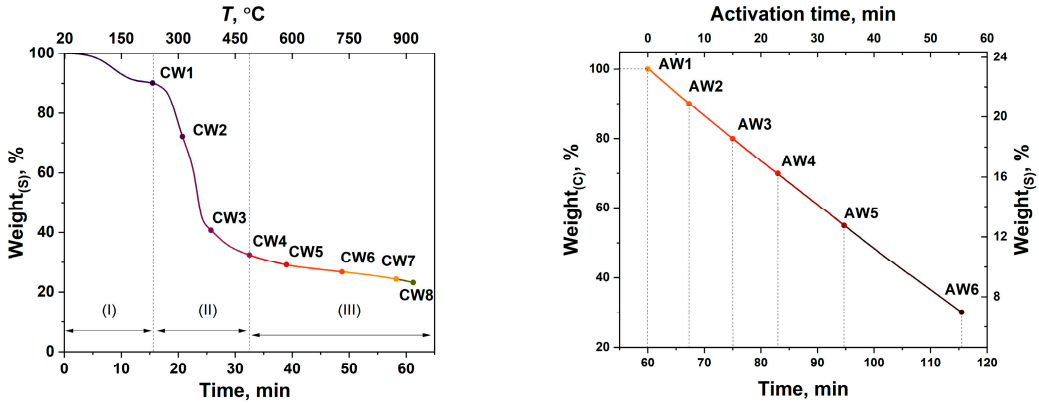

(**a**) (**b**)

Figure 2. Weight losses in the CW materials during the carbonization process (**a**) plotted as a function of the carbonization temperature (top axis) and duration of the entire synthesis (bottom axis), and weight losses in the AW materials during the activation (**b**) plotted versus the duration of the total synthesis (bottom axis) and the activation (top axis) processes. The vertical dashed lines in (**a**) indicate the regions corresponding to the stages in the formation of carbonizate (I), (II), and (III); the vertical lines in (**b**) show the evolution of carbonizate into activated carbons. Weight(s) is the mass of a sample with respect to the initial mass of the precursor (WNS); weight (C) is the mass of a sample with respect to the initial mass of the carbonizate prepared at 900 °C. The evolution in the color corresponds to an increase in the pyrolysis temperature (**a**) and burn-off degree (**b**) in accordance with Figure 1.

The examination of the weight losses of WNSs during carbonization (Figure 2a) revealed three characteristic ranges [2,19,21].

Region (I) corresponds to the dehydration of WNSs (removal of intracrystalline water) and the beginning of the pyrolysis of organic compounds present in the shells. When the sample was heated to a temperature of about 250 °C (CW1), the mass decreased by 8–10%.

Region (II) reflects the transformations of the sample starting at a temperature of 250–280 °C, which resulted in an abrupt mass loss of more than 40% (CW2, CW3). These dramatic changes in the TGA curves can be attributed to the decomposition of high-molecular compounds. The transformations occurring within region (II) are crucial for the yield product and characterize the quality of the precursor. The intensive mass loss occurred up to temperatures of 300–420 °C (CW2, CW3), and afterwards, the mass loss curve became flatter. At a temperature of 450–500 °C (CW4), the carbonization process started, and the material composition was enriched with carbon, which can be indicated as a transition to region (III).

Region (III) is characterized by the release of these products of the thermal decomposition of high-molecular components of WNSs, which filled the pores and became volatile. At 500–600 °C, the volatile compounds were removed from the forming carbon matrix. These processes mark the topochemical transformations occurring in the material (CW5 and CW6), where the primary regular pore structure was developed. Within a temperature range of 600–750 °C, the changes in the mass of the sample proceeded slowly. But when the temperature exceeded 800 °C (CW7 and CW8, Figure 2a), the rate of mass loss increased as the formation of primary porosity was completed. These temperatures corresponded to the beginning of the activation process, resulting in the development of the pore space directly in the carbon matrix.

When the pyrolysis process reached the isothermal activation stage at a temperature of 900 °C (AW1, Figure 2b), the residual mass of the carbonizate material in relation to the initial mass of the precursor was not more than 25%. The process of physical activation in the presence of CO_2 can be described by the following reaction:

$$2C + CO_2 \overset{900^\circ}{\rightarrow} C + 2CO, \quad (1)$$

As follows from Figure 2b, during the isothermal activation, the weight of the activated carbons linearly decreased with the activation time at a rate of 1.25% (mass)/min. The weight loss of the carbonizate during the activation process was ~70%. The total weight loss of the WNS precursor during the transformation into the final AW6 product was ~93%.

3.2. Adsorption Properties of WNS-Derived Carbon Materials

The development of the porosity in the carbon materials prepared from the WNSs that are crucial for adsorption properties can be followed by examining the isotherms of low-temperature nitrogen vapor adsorption recorded during the carbonization and activation processes, which are represented in Figure 3a and b, respectively.

According to Figure 3a, as the carbonization temperature rose, the adsorption capacity of the resulting materials increased, which points to the gradual development of porosity during the carbonization process. It should be noted that the processes of N_2 adsorption/desorption onto the CW1–CW3 materials were found to be irreversible. This fact indicates the presence of ultramicropores in these adsorbents and the encapsulation of nitrogen molecules in the pores. The absolute nitrogen adsorption onto these materials did not exceed 0.2 mmol/g. Therefore, as follows from the data for the CW1–CW3 samples, the carbonization of WNSs at temperatures below 500 °C resulted in the materials lacking microporosity.

At temperatures above 500 °C, the development of porosity proceeded more intensively due to the release of low-molecular volatile compounds (topochemical transformations) [2,18]. Indeed, only starting from the CW5 material, the carbonizates exhibited relatively high adsorption capacity, which ranged from 4 to 7 mmol/g, indicating the formation of a significant volume of micropores. The Γ-shaped isotherms (Type I according to the IUPAC classification [28]) of nitrogen adsorption onto the CW5 and CW6 materials are

specific for microporous carbon adsorbents. The isotherms of the CW7 and CW8 samples acquire a form close to the I (b) type according to the IUPAC classification [28], showing that these possess PSD over a broader range, including wider micropores and narrow mesopores.

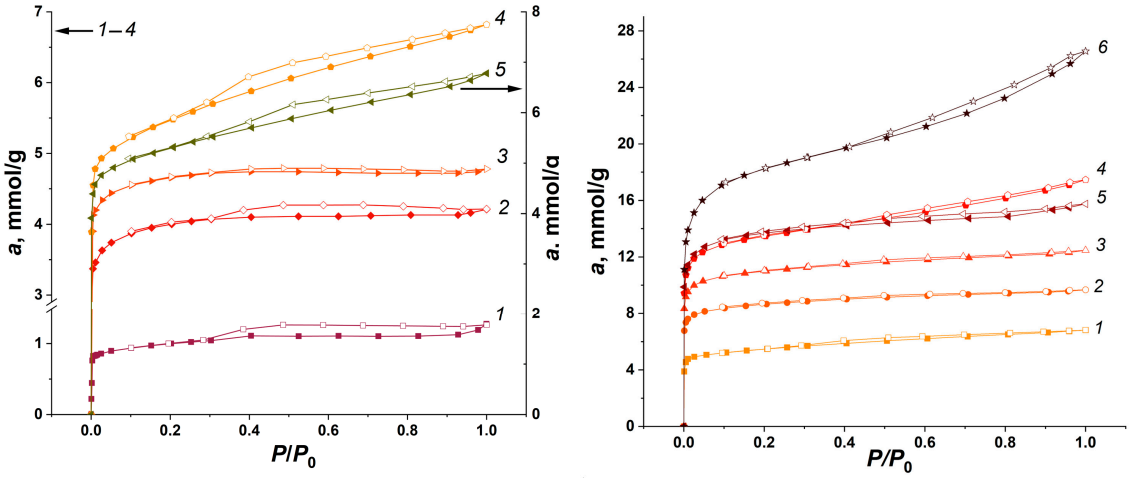

(**a**) (**b**)

Figure 3. (**a**) The N_2 adsorption (solid symbols)/desorption (open symbols) isotherms at 77 K for the carbon materials CW4 (1), CW5 (2), CW6 (3), CW7 (4), and CW8 (5) prepared from the WNS precursor by pyrolysis at temperature T_C, °C: 500, 600, 750, 900, and 950. (**b**) The N_2 adsorption (solid symbols)/desorption (open symbols) isotherms at 77 K for the carbon materials of the AW series, AW1/CW7 (1), AW2 (2), AW3 (3), AW4 (4), AW5 (5), and AW6 (6), with different burn-off degrees, %: 0, 10, 20, 30, 45, and 70. Symbols show the experimental data, and lines are the approximations.

As follows from Figure 2b, all the materials in the AW series exhibited the features of Type I isotherms of nitrogen adsorption, with a large uptake in the early stage of adsorption. The isotherms obtained for the carbon adsorbents with a burn-off degree exceeding 30%, i.e., for AW4–AW6 adsorbents, show a narrow hysteresis loop, which is indicative of the formation of supermicropores and transient narrow mesopores (I (b)-type according to the IUPAC). The data on the low-temperature N_2 vapor adsorption obtained for the carbon materials of both series were used for evaluating their structure and energy characteristics employing the Dubinin–Radushkevich (D-R) equation and BET equations for micropores and the Kelvin equation for mesopores. The calculated characteristics are provided in Table 1.

According to Table 1, microporosity started to develop in the CW samples only at temperatures above 500 °C. At a carbonization temperature ranging from 600 to 750 °C, the decomposition of high-molecular compounds was combined with a slight shrinkage of the carbon matrix [2,21], which manifested itself in an insignificantly altered micropore size and micropore volume. During carbonization at a temperature of 500 °C and above, in addition to micropores, mesopores were formed in a small amount. A rise in the carbonization temperature from 900 to 950 °C did not affect the adsorption capacity of the resulting carbon materials. However, it led to the intensive transformation of micropores to narrow mesopores as well as the burnout of the amorphous phase of carbon, resulting in a slight degradation of microporosity. The extended hysteresis loops on the adsorption isotherms obtained for the CW7 and CW8 samples (Figure 2a) were indicative of the presence of narrow transient mesopores, while the size and volume of micropores remained almost unchanged (see Table 1).

An increase in the burn-off degree of the AW adsorbents from 0 to 30% (AW1–AW4) was accompanied by a growth in their adsorption capacity caused by an almost two-fold increase in the micropore volume. The prolongation of the activation of carbonizate at 900

°C from 35 to 55 min increased the burn-off degree almost by half, which was accompanied by a noticeable increase in the microporosity and degradation of mesopores (see Table 1). During the activation process, which includes the consequent burning of the hexagonal carbon layers in graphite nanocrystallites, the average micropore size increased, reducing the characteristic energy of adsorption (see Table 1). The evolution of the porous system of carbon materials during the activation stage can be followed by examining the pore size distribution (PSD) in several carbon adsorbents of the AW series represented in Figure 4.

Table 1. The structure and energy characteristics of the adsorbents of the CW and AW series calculated from the low-temperature nitrogen vapor adsorption at 77 K.

Sample	Micropores			Mesopores			W_S, cm^3/g	δ [1], mass.%	T_C/T_A, °C
	W_0, cm^3/g	E_0, kJ/mol	x_0, nm	S_{BET}, m^2/g	W_{meso}, cm^3/g	S_{meso}, m^2/g			
CW1	0	0	0	0	0	0	0	10	240/-
CW2	0	0	0	0	0	0	0	18	320/-
CW3	0	0	0	0	0	0	0	60	400/-
CW4	0.03	28.7	0.42	80	0.01	0	0.04	68	500/-
CW5	0.14	26.7	0.45	310	0.01	0	0.15	71	600/-
CW6	0.16	26.1	0.45	360	0.01	0	0.17	73	750/-
CW7/AW1	0.19	26.2	0.46	430	0.05	0	0.24	75/0	900/900
CW8	0.18	25.5	0.47	410	0.05	0	0.23	77	950/-
AW2	0.29	27.8	0.43	680	0.05	21	0.34	10	-/900
AW3	0.37	25.9	0.46	860	0.05	21	0.43	20	-/900
AW4	0.45	23.2	0.52	1060	0.06	41	0.61	30	-/900
AW5	0.47	22.2	0.54	1070	0.16	86	0.55	45	-/900
AW6	0.60	19.7	0.61	1440	0.09	60	0.92	70	-/900

[1] δ is the burn-off determined for the CW and AW adsorbents with respect to the weight of the initial WNS precursor and the carbonizate prepared at 900 °C, respectively. For the CW7/AW1 adsorbent, δ = 75/0%.

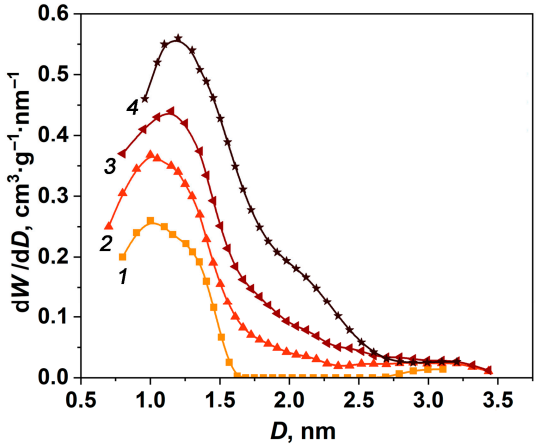

Figure 4. Pore size distribution calculated by the QSDFT method based on the low-temperature nitrogen vapor adsorption in AW series carbon materials: AW1 (1), AW3 (2), AW5 (3), and AW6 (4).

As seen from Figure 4, the elongation of the physical activation of carbonizates led to the expansion of micropores, including those corresponding to a peak of PSD from 1.0 to 1.25 nm, and an increase in their volume. The increase in the burn-off of the activated carbons led to the development of both narrow and wide micropores within a range of 1.0 to ~3.5 nm, which manifested itself in an increase in the width of the PSD function and the area under the PSD curve. It should be noted that the AW5 sample resulting from the activation at 900 °C during 95 min possessed a BET surface and micropore volume close to those reported for the carbon material prepared by Lionetti with coworkers by the activation at the same temperature during 90 min: 1163 m^2/g and 0.45 cm^3/g, respectively [18].

3.3. X-ray Analysis of Prepared Adsorbents

X-ray diffraction allows for a structural analysis of the samples. Figure 5a,b provide the possibility to examine the effect of the carbonization temperature (a) and the degree of burn-off determined by the activation time (b) on the morphological features of the resulting carbon materials.

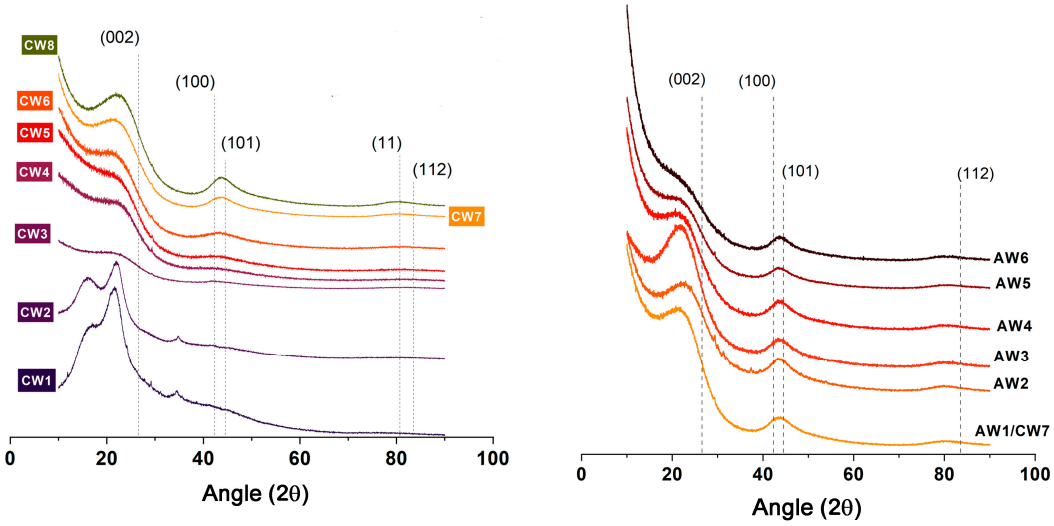

Figure 5. XRD patterns recorded for the carbon materials of the CW (**a**) and AW (**b**) series.

The XRD patterns for CW1 and CW2 show two broad peaks at 2θ = 17° and 22° and one narrow peak at 2θ = 34° (see Figure 5a), which are attributed to the reflections of partially disordered cellulose I [29] inherited from the raw material [30]. The XRD patterns for the CW3–CW5 materials (pyrolysis at a carbonization temperature ranging from 400 to 600 °C) show very broad diffraction peaks typical for amorphous sp^2 carbon. As the carbonization temperature rises up to 750 °C and higher (CW6–CW8), there is a gradual increase in the intensity of reflections above the background, which is interpreted as the formation of nanosized and highly ordered graphite-like crystallites. After the treatment of WNSs at a carbonization temperature of 900–950 °C (CW7 and CW8), both the relative fraction and the quality of these crystallites increased.

The samples AW1/CW7–AW3 with a burn-off degree ranging from 0 to 20% (see Figure 5b) contained a relatively high fraction of graphitic nanocrystals embedded in disordered carbon. At a burn-off degree of 20% (AW3), the graphite 002 reflection markedly increased in intensity, while its half-width remained unchanged. Based on the Scherrer formula (note that it should be used with caution in this case [31]), we found that the height of the stacked graphene layers was close to 1 nm, and the lateral size of these crystallites, which was about 1.7 nm, remained almost constant during the activation process. The observed behavior of diffraction patterns can be explained on the assumption that the lateral size of the staked graphite structures corresponds to a diameter of graphitized cellulose fibrils, and the increase in the intensity of the 002 reflection while maintaining its half-width indicates the ordering of individual graphene stacks along the axis inherited from initial cellulose fibrils. Interestingly, for the later sample, the patterns obtained for fully dried and wet material differ notably: for the wet sample, 002 is weaker, implying a higher curvature of the precursor fibril. Note that for other active carbons, contrasting behavior may be observed [32].

Starting from the carbon materials with a burn-off degree of 30% (AW4), the intensity of the 002 reflection decreased due to the accumulation of interlayer defects, while the lateral size of crystallites changed insignificantly. Probably, cellulose nanofibrils were

completely destroyed, with an accompanying disorder of the spatial arrangement of the graphene stacks.

Figure 6a,b show the SAXS curves for the CW and AW series, respectively, in a log–log representation.

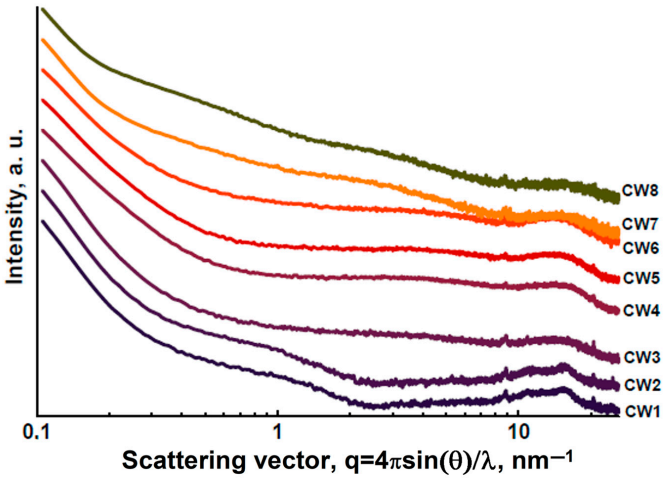

(**a**)

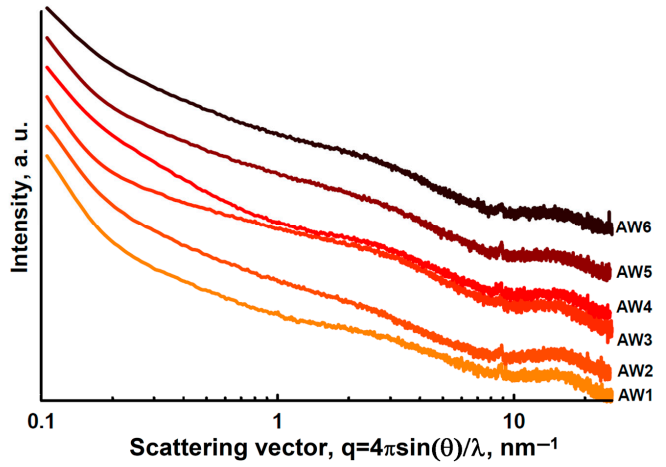

(**b**)

Figure 6. Small-angle X-ray scattering from carbonizates of CW series prepared at different carbonization temperatures (**a**) and activated carbon materials of AW series with different burn-off degrees (**b**).

The log–log plots of the scattering intensity I against the scattering vector q ($q = 4\pi\sin(\theta)/\lambda$, nm^{-1}) for almost all the adsorbents are typical for scattering from the hierarchical structures, those comprising two populations of heterogeneities, which differ significantly in sizes: 15–20 nm (large crystals) and a few nanometers or less (micropores). The population of large particles was found in all the samples of carbon materials; however, the size and relative fraction of small heterogeneities depended on the carbonization temperature. The linearity of the Guinier plots allowed us to calculate the radius of gyration of a cross-section of micropores, R_G, using the Guinier formula in a linear form for three models of pore shape: spherical, slit-like, and cylindrical.

The results of the calculations for the carbon materials of the CW and AW series are listed in Tables 2 and 3, respectively, in which they can be compared with the pore sizes evaluated from the low-temperature adsorption data.

Table 2. The textural characteristics of the carbonizates (CW series), including the standard characteristic energy of adsorption and the half-width of micropores calculated from the low-temperature N_2 adsorption data, and the radii of gyration of micropores calculated from the SAXS data based on the model of slit-like pores.

Sample	E_0, kJ/mol	x_0, nm	R_G	T_C, K
CW1	no micropores	0	1.17	240
CW2	no micropores	0	1.45	320
CW3	no micropores	0	*	400
CW4	35.3	0.34	*	500
CW5	22.2	0.54	*	600
CW6	25.1	0.46	*	750
CW7	26.7	0.45	0.47	900
CW8	25.5	0.47	0.50	950

* None of the models for pore shape gave a reasonable value of the radius of gyration.

Table 3. The textural characteristics of the carbon materials activated at 900 °C (AW series), including the standard characteristic energy of adsorption and half-width of micropores calculated from the low-temperature N_2 adsorption data and the radii of gyration of micropores calculated from the SAXS plots based on the models of the slit-like (R_G), spherical (R_{GS}), and cylindric (R_{GC}) pore shapes.

Sample	E_0, kJ/mol	x_0, nm	R_G, nm	R_{GS}, nm	R_{GC}, nm	δ, %
AW1	26.2	0.46	0.440	0.570	*	0
AW2	27.8	0.43	0.496	0.641	0.376	10
AW3	25.9	0.46	0.457	0.590	0.280	20
AW4	23.2	0.52	0.486	0.627	0.235	30
AW5	22.2	0.54	0.304	0.393	0.317	45
AW6	19.7	0.61	0.475	0.614	0.346	70

* The model of cylindric pores did not give a reasonable value of the radius of gyration.

In CW1 and CW2, which were prepared at the lowest temperatures of 240 and 320 °C, a weak scattering of X-rays from the heterogeneities with a size of 1–1.5 nm was observed. The SAXS curve was well described under the assumption of a cylindrical shape for heterogeneities (with a size of 2 nm). Taking into account the absence of microporosity in these samples (see Table 1), the scattering can be attributed not to pores but to other types of heterogeneities, for example, defects in partially carbonized fibrils of cellulose, which is an essential component of the shells [31]. Note that the partially carbonized cellulose fibrils were identified in the XRD patterns (see Figure 5a).

With the rising temperature of carbonization, the contribution from this type of heterogeneity was replaced by a very weak scattering from the objects with a size of 0.5–1.0 nm, which can be assigned to micropores. In CW3, the contribution from micropores was very small. Despite the qualitative similarity of the SAXS curves between CW3, CW4, and CW5, their analysis showed that an increase in the carbonization temperature led to an increase in the fraction of micropores. When the temperature of carbonization rose up to 750 °C, the hierarchical structure of the material became more pronounced (see curve for CW6), although the proportion of pores remained small. In the samples CW7 and especially CW8, scattering from pores became quite strong. Moreover, the analysis of the SAXS curves for these materials revealed the presence of two types of heterogeneities, especially in CW8, where an additional increase in the scattering intensity at q~0.5 nm^{-1} was observed.

When examining the SAXS data for the activated carbons (AW series) in Figure 6b, one can observe a region that corresponds to the scattering from the pore observed at q ranging from 2 to 8 nm^{-1}. A comparison of the SAXS curves of the materials with different burn-off degrees within a range of q of 0.3 to 1.0 nm^{-1} points to noticeable distinctions in the structure on scales of the order of 6–18 nm^{-1}. Although an unambiguous explanation of the differences is impossible without additional information, the comparison of the SAXS and XRD data provides the possibility to suggest that the change in the course of the curves with increasing burn-off degrees (see curves for AW3 and AW4 in Figure 6b) can be

related to the destruction of graphitized nanofibrils of cellulose and the complete structural rearrangement occurring during the activation processes.

3.4. Raman Spectroscopy Data for Carbon Adsorbents

Raman spectroscopy is a widely used method for disclosing crystallographic disorders in porous carbons [27,32]. Figure 7 shows the Raman spectra for the CW and AW materials. The usual practice of processing Raman spectra involves decomposing the envelope contour of the spectrum into components. Although the spectrum in the single-phonon region can be fitted by four components (D, G, A, and T) [33], the difference curve indicates the need to introduce a fifth component with a larger half-width than the D-component but at a position close to its peak.

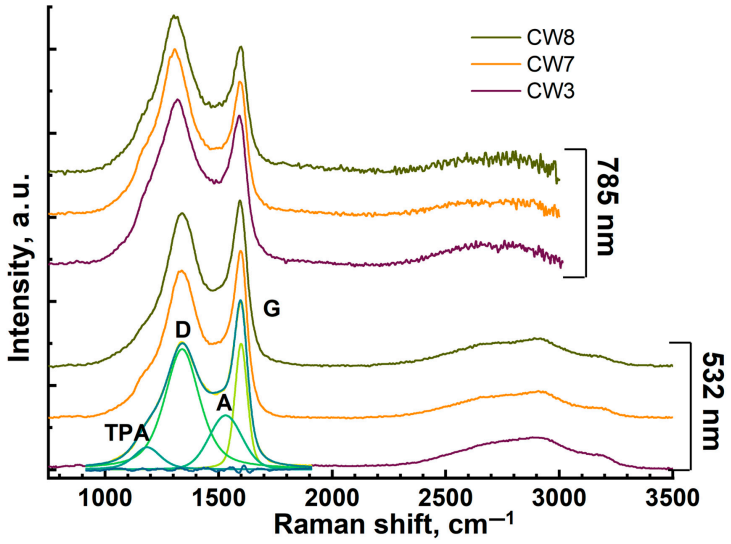

(a)

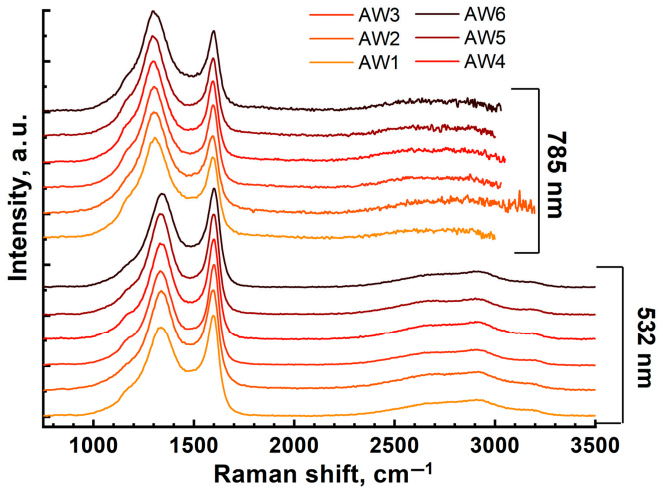

(b)

Figure 7. *Cont.*

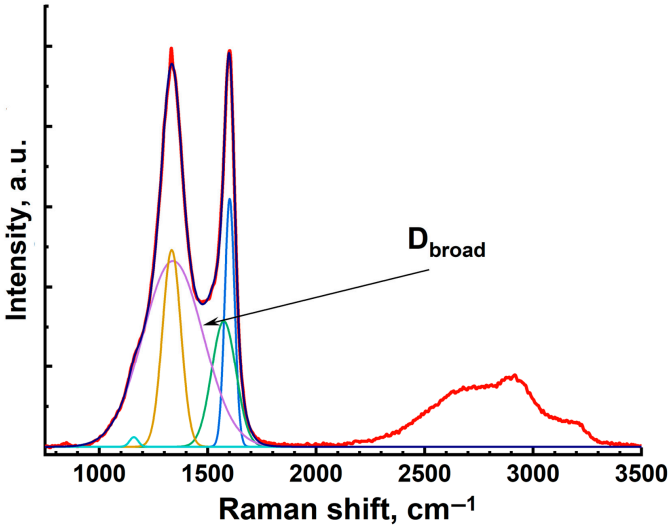

(**c**)

Figure 7. The first- and second-order Raman spectra for the CW (**a**) and AW (**b**) carbon materials, and the decomposition of the first-order spectrum for AW4 into five components shown as an example (**c**). The curves are vertically shifted for clarity. The excitation wavelength is shown on the right.

From our point of view, the use of an additional component is not just a mathematical exercise but is based on the complex structure of the WNS precursor, which includes both cellulose and lignin. Since the carbonization of these compounds proceeds at different rates, we expected to observe a noticeable heterogeneity in the structure of each carbon material. One can assume that carbonized cellulose made the main contribution to the narrow G- and D-bands, while the broad A- and D_{broad}-bands can be assigned to the carbonization products of lignin, which is a complex polyphenolic polymer.

The Raman spectra of the CW1–CW2 carbon materials are not provided in Figure 7a since they are not informative due to the exceptionally strong photoluminescence observed even when excited at a wavelength of 785 nm. The reason is the intrinsic photoluminescence of disordered (amorphous) sp^2 carbon with a wide band gap distribution. The spectra for other CW samples are typical for graphite-like adsorbents (see Figure 7a).

Figure 8 shows the spectroscopic parameters of both G- and A-bands, represented as a dependence of the peak position and its full-width at half maximum (FWHM) for the carbon materials produced by the carbonization of the WNS precursor (CW3–CW8) and the activation (AW1–AW6).

Figure 8 shows that in the case of the G-band, the points crowd around a position of the peak at 1590–1600 cm^{-1} cm and a half-width of 80 cm^{-1}. The coordinates of this group and general trend are in accordance with the data for hydrogen-containing amorphous carbon (a-C:H) materials [27,32,34]. However, the A-band exhibited significantly distinct behavior, especially in spectra recorded at the excitation wavelength of 785 nm. Although some of the samples are close to the common (a-C:H) trend, other behaviors are also observed: the peak position and the FWHM parameter ranged from 1520 to 1540 cm^{-1} and from 60–90 cm^{-1} to 1550–1560 cm^{-1} and 120 cm^{-1}, respectively. Such an effect was recently observed for activated carbons prepared from raw polymer materials, namely furfural [27]. This similarity indirectly confirms the assumption that, with high probability, the A-band can be assigned to the products of the carbonization of lignin. Such materials are characterized by a high degree of graphite disorder and the presence of defective carbon cycles.

Figure 9 shows the correlation between the intensities of the D- and G-bands, $I(D)/I(G)$, and their analogs for lignin, D_{broad} and A, and the specific BET surface, which is determined by the carbonization temperature and the burn-off degree.

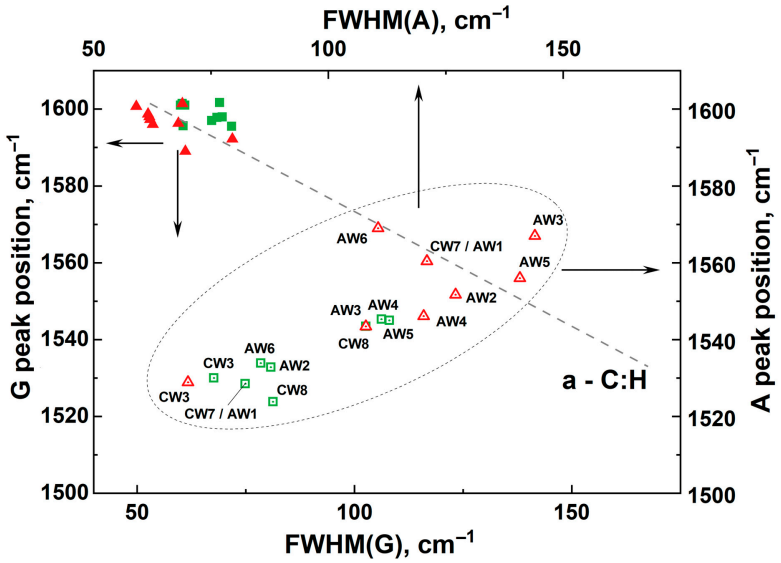

Figure 8. The dependence of the positions of the G- (solid symbols, left and bottom axes) and A-peaks (right and top axes, open symbols) on their FWHM parameters at the excitation wavelength of 532 nm (green symbols) and 785 nm (red symbols) for CW3–CW8 and AW1/CW7–AW6.

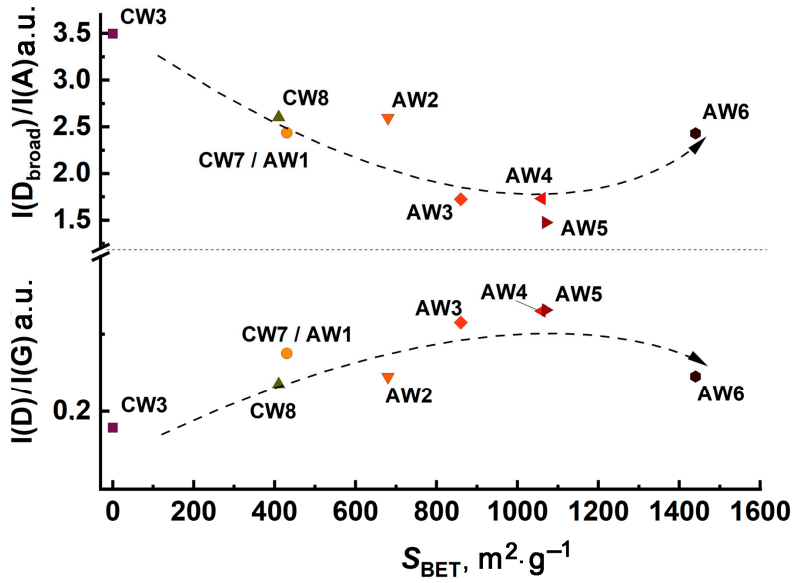

Figure 9. The ratio of intensities of the D- and G-peaks, I(D)/I(G) (bottom), and their analogs, $I(D_{broad})/I$(A) (top), versus specific BET surfaces, which depend on the burn-off degree. The dashed lines indicate the trend of the changes in the intensity ratios with an increase in the burn-off degree.

As follows from the figure, there is a significant difference between the behaviors demonstrated by I(D)/I(G) attributed to the products of the carbonization of cellulose with an increase in S_{BET} (or δ) and that for carbonized lignin. In the case of carbonized cellulose, at first, the intensity ratio increases moderately, reaching a maximum, and then it gradually decays, while for carbonized lignin, one can observe the opposite effect: the initial decay of the intensity ratio to a minimum is followed by its growth. Although the ratio I(D)/I(G) is often used to estimate the crystallite size, the deep analysis carried out by Schuepfer and coworkers [35] revealed that the same value of this ratio can correspond to crystallites of significantly different sizes. This incongruity was explained by different mechanisms of signal occurrence (Raman scattering and diffraction). Therefore, to avoid

incorrect conclusions, we did not evaluate the sizes of crystallites based on the Raman spectroscopy data.

An increase in the carbonization temperature and the activation time (or the burn-off degree) also led to a clear decomposition of the second-order spectrum (2500–3300 cm^{-1}). For all the carbon materials, the relative intensity of the D-band in the spectra obtained at the excitation wavelength of 785 nm is higher than in those obtained at 532 nm. In all cases, we observed a negative dispersion of the position of the D-peak calculated as follows:

$$[\sigma G(\lambda_1) - \sigma G(\lambda_2)]/[\lambda_1 - \lambda_2], \text{ here} \lambda_1 = 785\text{nm} \text{and} \lambda_1 = 532\text{nm} \quad (2)$$

The position of the D-peak is shifted from the wave number of 1340 cm^{-1}, which is typical for a perfect graphite crystal at the laser excitation wavelength of 532 nm, towards smaller numbers. We attributed this effect to the tensile stresses in graphite-like materials.

Figure 10a,b illustrate the correlation between the intensity ratio of the A- and G-bands and the porosity parameters determined from the nitrogen adsorption data.

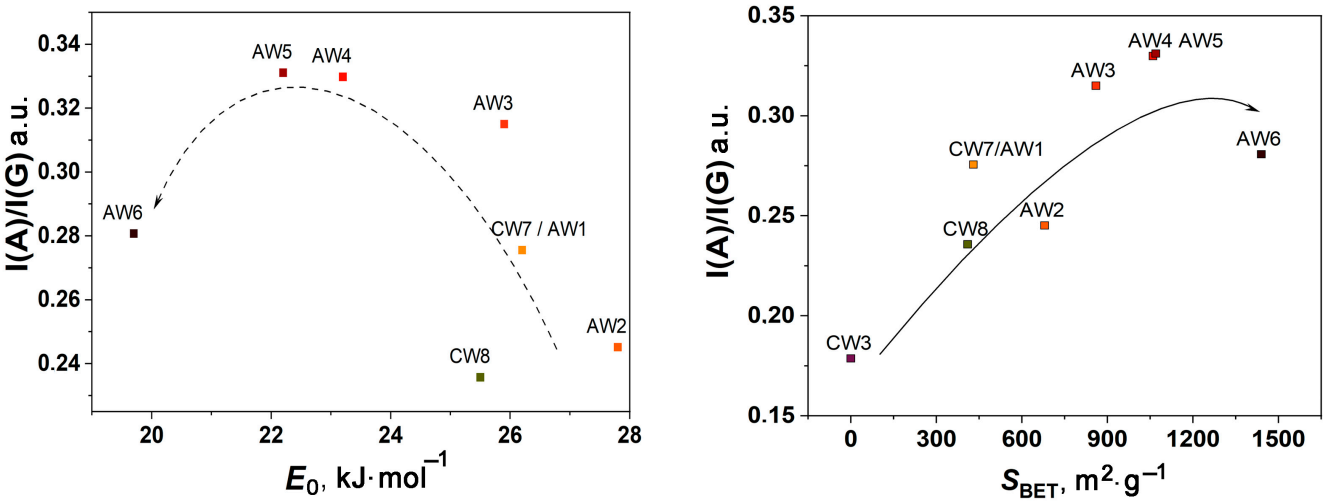

Figure 10. The ratio of the intensities of the A- and G-peaks, $I(A)/I(G)$, versus the characteristic energy of adsorption (**a**) and specific BET surface (**b**). The lines indicate the qualitative correlation trends with an increase in the burn-off degree.

Both figures show a growth in the relative intensity of the A-band with an increase in porosity. But at the maximum burn-off degrees, the trend changes direction. It should be noted that we observed the opposite dependence for a series of activated carbons of various genesis [27], based on which we assumed that the A-peak corresponded to the amorphous component of the material, which blocked the access of gas molecules to ultra- and supermicropores [27,32]. The effects observed in the present study allowed us to assume that, unlike previously studied activated carbons prepared from furfural, bitumen, and various wood waste, in WNS carbonization products, the amorphous phase inherited from lignin is spatially separated from graphitized cellulose fibrils, whose porosity determines the adsorption capacity of the carbon materials.

4. Conclusions

In order to analyze the process of the formation of the porous structure of carbon materials during the carbonization of WNSs in CO_2 flow at temperatures up to 950 °C, two series of carbon materials were prepared in the furnace of the TGA instrument, which differed in the carbonization temperature (CW series) and activation time (AW).

The analysis of the porous structure of the CW materials showed that the pore formation started at the carbonization temperature of 500 °C, which can be considered the

minimum possible threshold for preparing nanoporous adsorbents from the WNS precursor. In general, the continuous heating of the raw material without holding it at a certain carbonization temperature does not produce adsorbents with a developed porosity. The largest micropore volume and specific BET surface achieved at 900 °C carbonization temperature were only 0.19 cm^3/g and 430 m^2/g, respectively.

The activation of the CW materials by holding at 900 °C in CO_2 flow for various time intervals produced a series of AW1–AW6 adsorbents with a developed microporosity and relatively narrow pore size distribution within a range of 1.0 to 1.25 nm. When the CW material was kept until the burn-off degree reached 70%, the mesopores emerged and contributed significantly to the overall porosity of the resulting adsorbent.

The structural transformations of the raw material during carbonization, followed by the changes in its carbonizate caused by the activation process, were examined via an analysis of the XRD data. An examination and comparison of the XRD patterns made it possible to identify the carbonization temperature range within which the amorphous sp^2 carbon was formed (400–600 °C), while an increase in the intensity of the corresponding reflections observed at 750 °C was caused by the formation of nanosized, ordered graphite-like crystallites surrounded by disordered carbon phase. With the carbonization temperature rising to 900–950 °C, the fraction and quality of the graphite-like crystallites grew. The activation of carbonizate, which was accompanied by an increase in the burn-off degree to 30%, led to interlayer defects, resulting in an intensity attenuation of the (002) reflection. A decrease in the coherent scattering region and an increase in the background corresponding to disordered carbon, which were observed in the materials with higher burn-off degrees, indicated pore formation in crystallites, resulting from the destruction of cellulose nanofibrils and the disordering of graphite stacks.

Two populations of heterogeneities of different dimensions assigned to large crystallites and micropores determine the SAXS curves for all the carbon materials under study. No correlation was found between the radius of gyration of micropores calculated using three models of pore shapes and the pore characteristics evaluated from the adsorption data.

In terms of Raman spectroscopy, all the products of carbonization and activation can be classified as a broad class of amorphous hydrogen-containing carbon materials. A combined analysis of the XRD patterns, SAXS curves, and Raman spectra revealed a significant effect of the WNS precursor, composed of cellulose fibrils, which are surrounded by lignin, on the final structure of carbonizate. In the initial stages of carbonization, this structure was preserved, and the graphitized cellulose fibrils were spatially separated from the lignin phase. The multiphase composition of the carbon materials required us to decompose the Raman spectra into components. The analysis of these components showed that the main fraction of pores, which are accessible for gas molecules, are located in the phase of graphitized cellulose fibrils, whereas the contribution from graphitized lignin is insignificant.

In conclusion, the preparation of activated carbons from walnut shells through the one-stage activation process in CO_2 flow has the advantage that it makes it possible to obtain carbon adsorbents with relatively uniform porosity, which can be regulated by the carbonization temperature and the activation time, for wide applications, including gas storage and separation.

Author Contributions: Conceptualization, I.E.M., A.V.S. and A.A.F.; methodology, I.E.M., A.A.S. and A.A.A.; software, A.E.G.; validation, A.A.S., A.A.A. and A.A.F.; formal analysis, A.A.S., A.A.A. and A.E.G.; investigation, I.E.M., A.A.S. and A.A.A.; resources, A.V.S. and A.A.S.; data curation, A.A.F.; writing—original draft preparation, I.E.M., A.A.S. and A.A.A.; writing—review and editing, A.A.F. and E.V.K.; visualization, A.E.G. and E.V.K.; supervision, I.E.M.; project administration, A.A.F.; funding acquisition, A.A.F. All authors have read and agreed to the published version of the manuscript.

Funding: This research was funded by the Ministry of Science and High Education of the Russian Federation, the State task no. 122011300053-8.

Data Availability Statement: The data supporting the findings of the study are presented within this study.

Acknowledgments: All the experiments were carried out using equipment of the Center of Physical Methods of Investigations of the A.N. Frumkin Institute of Physical Chemistry and Electrochemistry of the Russian Academy of Sciences.

Conflicts of Interest: The authors declare no conflicts of interest.

References

1. Agroinvestor. Available online: https://www.agroinvestor.ru/markets/news/30896-dolya-rossii-v-mirovom-sbore-orekhov-ne-prevyshaet-1/ (accessed on 10 December 2023).
2. Fenelonov, V.B. *Poristyi Uglerod (Porous Carbon)*; Boreskov Institute of Catalysis SB RAS: Novosibirsk, Russia, 1995; p. 518. (In Russian)
3. Mukhin, V.M.; Tarasov, A.V.; Klushin, V.N. *Aktivnie Ugli Rossii (Active Carbons of Russia)*; Metallurgiya: Moscow, Russia, 2000; p. 352.
4. Wartelle, L.H.; Marshall, W.E. Nutshells as Granular Activated Carbons: Physical, Chemical and Adsorptive Properties. *J. Chem. Technol. Biotechnol.* **2001**, *76*, 451–455. [CrossRef]
5. Lupascu, T.; Dranca, I.; Popa, V.T.; Vass, M. Application of Thermal Analysis to the Study of Some Waste Agricultural Products for the Preparation of Active Carbons. *J. Therm. Anal. Calorim.* **2001**, *63*, 855–863. [CrossRef]
6. González, J.F.; Román, S.; González-García, C.M.; Nabais, J.M.N.; Ortiz, A.L. Porosity Development in Activated Carbons Prepared from Walnut Shells by Carbon Dioxide or Steam Activation. *Ind. Eng. Chem. Res.* **2009**, *48*, 7474–7481. [CrossRef]
7. Nowicki, P.; Pietrzak, R.; Wachowska, H. Sorption properties of active carbons obtained from walnut shells by chemical and physical activation. *Catal. Today* **2010**, *150*, 107–114. [CrossRef]
8. Bae, W.; Kim, J.; Chung, J. Production of granular activated carbon from food-processing wastes (walnut shells and jujube seeds) and its adsorptive properties. *J. Air Waste Manag. Assoc.* **2014**, *64*, 879–886. [CrossRef]
9. Serafin, J.; Dziejarski, B.; Cruz, O.F., Jr.; Sreńscek-Nazzal, J. Design of highly microporous activated carbons based on walnut shell biomass for H_2 and CO_2 storage. *Carbon* **2023**, *201*, 633–647. [CrossRef]
10. Li, X.; Qiu, J.; Hu, Y.; Ren, X.; He, L.; Zhao, N.; Ye, T.; Zhao, X. Characterization and comparison of walnut shells-based activated carbons and their adsorptive properties. *Adsorpt. Sci. Technol.* **2020**, *38*, 450–463. [CrossRef]
11. Serafin, J.; Dziejarski, B. Activated carbons-preparation, characterization and their application in CO_2 capture: A review. *Environ. Sci. Pollut. Res. Int.* **2024**, *31*, 40008–40062. [CrossRef]
12. Yang, L.; Yungang, W.; Tao, L.; Li, Z.; Yanyuan, B.; Haoran, X. High-performance sorbents from ionic liquid activated walnut shell carbon: An investigation of adsorption and regeneration. *RSC Adv.* **2023**, *13*, 22744–22757. [CrossRef]
13. Yu, Q.; Li, M.; Ning, P.; Yi, H.; Tang, X. Preparation and Phosphine Adsorption of Activated Carbon Prepared from Walnut Shells by KOH Chemical Activation. *Sep. Sci. Technol.* **2014**, *49*, 2366–2375. [CrossRef]
14. Kim, J.-W.; Sohn, M.-H.; Kim, D.-S.; Sohn, S.-M.; Young-Shik Kwon, Y.-S. Production of granular activated carbon from waste walnut shell and its adsorption characteristics for Cu^{2+} ion. *J. Hazard. Mater.* **2001**, *85*, 301–315. [CrossRef]
15. Yang, J.; Qiu, K. Preparation of Activated Carbons from Walnut Shells via Vacuum Chemical Activation and Their Application for Methylene Blue Removal. *Chem. Eng. J.* **2010**, *165*, 209–217. [CrossRef]
16. Zabihi, M.; Asl, A.H.; Ahmadpour, A. Studies on adsorption of mercury from aqueous solution on activated carbons prepared from walnut shell. *J. Hazard. Mater.* **2010**, *174*, 251–256. [CrossRef] [PubMed]
17. Albatrni, H.; Qiblawey, H.; Al-Marri, M.J. Walnut shell based adsorbents: A review study on preparation, mechanism, and application. *J. Water Process Eng.* **2022**, *45*, 102527. [CrossRef]
18. Lionetti, V.; Bonaventura, C.P.; Conte, G.; Luca, O.D.; Policicchio, A.; Caruso, T.; Desiderio, G.; Papagno, M.; Agostino, R.G. Production and physical-chemical characterization of walnut shell-derived activated carbons for hydrogen storage application. *Int. J. Hydrogen Energy* **2024**, *61*, 639–649. [CrossRef]
19. Liu, Y.; Wang, Y.; Zou, L.; Bai, Y.; Xiu, H. Research on the optimum carbonization process of walnut shell based on dynamic analysis. *RSC Adv.* **2023**, *13*, 13412–13422. [CrossRef] [PubMed]
20. *GOST 8050–85*; Carbon Dioxide Gaseous and Liquid. Technical Conditions. M. Izd-vo Standartov, Russian Federation: Moscow, Russian, 1995.
21. Men'shchikov, I.E.; Fomkin, A.A.; Romanov, Y.A.; Kiselev, M.R.; Pulin, A.L.; Chugaev, S.S.; Shkolin, A.V. Carbon Nanoporous Adsorbents Prepared from Walnut Shell for Liquefied Natural Gas Vapor Recovery in Cryogenic Storage Systems. *Prot. Met. Phys. Chem. Surf.* **2020**, *56*, 1122–1133. [CrossRef]
22. Dubinin, M.M. Physical adsorption of gases and vapors in micropores. *Prog. Surf. Membr. Sci.* **1975**, *9*, 1–70.
23. Brunauer, S.; Emmett, P.H.; Teller, E. Adsorption of gases in multimolecular layers. *J. Am. Chem. Soc.* **1938**, *60*, 309–319. [CrossRef]
24. Gregg, S.J.; Sing, K.S.W. *Adsorption, Surface Area and Porosity*; Academic Press: London, UK; New York, NY, USA, 1982.
25. Neimark, A.V.; Lin, Y.; Ravikovitch, P.I.; Thommes, M. Quenched Solid Density Functional Theory and Pore Size Analysis of Micro-Mesoporous Carbons. *Carbon* **2009**, *47*, 1617–1628. [CrossRef]

26. Men'shchikov, I.; Shiryaev, A.; Shkolin, A.; Vysotskii, V.; Khozina, E.; Fomkin, A. Carbon adsorbents for methane storage: Genesis, synthesis, porosity, adsorption. *Korean J. Chem. Eng.* **2021**, *38*, 276–291. [CrossRef]
27. Shiryaev, A.A.; Pré, P.; Pardanaud, C.; Murzin, V.; Averin, A. Microporosity and nanostructure of activated carbons: Characterization by X-ray diffraction and scattering, Raman spectroscopy and transmission electron microscopy. *Adsorption* **2023**, *29*, 275–289. [CrossRef]
28. Thommes, M.; Kaneko, K.; Neimark, A.V.; Oliver, J.P.; Rodrigues-Reinoso, F.; Rouquerol, J.; Sing, K. Physisorption of gases, with special reference to the evaluation of surface area and pore size distribution (IUPAC Technical Report). *Pure Appl. Chem.* **2015**, *87*, 1051–1069. [CrossRef]
29. French, A.D. Idealized powder diffraction patterns for cellulose polymorphs. *Cellulose* **2014**, *21*, 885–896. [CrossRef]
30. Xiao, N.; Felhofer, M.; Antreich, S.J.; Huss, J.C.; Mayer, K.; Singh, A.; Bock, P.; Gierlinger, N. Twist and lock: Nutshell structures for high strength and energy absorption. *R. Soc. Open Sci.* **2021**, *8*, 210399. [CrossRef] [PubMed]
31. Rutman, A.M.; Skakov, Y.A. Radial distribution functions of atoms and interference functions of partly ordered carbon materials. I. Influence of edge atoms of disperse layers. *Sov. Phys. Cryst.* **1989**, *34*, 338–341.
32. Shiryaev, A.A.; Voloshchuk, A.M.; Volkov, V.V.; Averin, A.A.; Artamonova, S.D. Nanoporous active carbons at ambient conditions: A comparative study using X-ray scattering and diffraction, Raman spectroscopy and N2 adsorption. *J. Phys. Conf. Ser.* **2017**, *848*, 012009. [CrossRef]
33. Merlen, A.; Buijnsters, J.G.; Pardanaud, C. A Guide to and Review of the Use of Multiwavelength Raman Spectroscopy for Characterizing Defective Aromatic Carbon Solids: From Graphene to Amorphous Carbons. *Coatings* **2017**, *7*, 153. [CrossRef]
34. Ferrari, A.C.; Robertson, J. Interpretation of Raman spectra of disordered and amorphous carbon. *Phys. Rev. B* **2000**, *61*, 14095–14107. [CrossRef]
35. Schuepfer, D.B.; Badaczewski, F.; Guerra-Castro, J.M.; Hofmann, D.M.; Heiliger, C.; Smarsly, B.; Klar, P.J. Assessing the structural properties of graphitic and non-graphitic carbons by Raman spectroscopy. *Carbon* **2020**, *161*, 359–372. [CrossRef]